PHYSICAL REVIEW B **78**, 245318 (2008)

First-principles investigation of the atomic and electronic structure of the 4*H*-SiC(1$\bar{1}$02)-*c*(2×2) surface

Björn Baumeier,* Peter Krüger, and Johannes Pollmann
Institut für Festkörpertheorie, Westfälische Wilhelms-Universität Münster, D-48149 Münster, Germany
(Received 29 September 2008; published 24 December 2008)

We present results of a comprehensive *ab initio* investigation of the atomic and electronic structure of a variety of reconstruction models for the 4*H*-SiC(1$\bar{1}$02)-*c*(2×2) surface. The basic structural building blocks are Si adatoms residing in *H*3 or *T*4 sites above the surface and carbon dimers in the top layer, respectively. These reduce the number of surface dangling bonds per unit cell from twelve at the ideal surface to only two in the different reconstruction models investigated. Several arrangements of triple-bonded carbon dimers bridging two second-layer Si atoms or double-bonded carbon dimers are considered. A configuration with double-bonded carbon dimer pairs and Si adatoms in *H*3 sites turns out to be most favorable. It is 2.1 eV per unit cell lower in total energy than the reconstruction model suggested earlier solely on the basis of experimental data. A reaction pathway of the surface from an initial configuration with Si adatoms in metastable *T*4 sites to the final adsorption configuration with Si adatoms in the most stable *H*3 sites is investigated, revealing an energy barrier of about 0.4 eV between the two. The electronic structure of several reconstruction models is analyzed by calculated surface band structures, charge-density distributions, and scanning tunneling microscopy images. The results are discussed in comparison with most recent experimental data.

DOI: 10.1103/PhysRevB.78.245318 PACS number(s): 68.35.bg, 73.20.At, 68.43.Fg, 68.35.Md

I. INTRODUCTION

Silicon carbide (SiC) is a compound semiconductor of large fundamental interest and high application potential.[1–3] Its cubic and hexagonal polytypes have wide band gaps and a very high thermal stability, making SiC especially suitable for high-temperature, high-frequency, high-power, high-voltage, and high-speed electronic devices and sensors.[4] Additional characteristics of SiC are its chemical inertness and very high hardness, qualifying it as an especially attractive material to operate under harsh environmental conditions.[5] Furthermore, SiC is one of the best biocompatible materials, very promising for biophysics applications.[6–8]

Among the key issues for practical microelectronics devices are high-quality SiC surfaces with a low defect density. There exist a lot of cubic *or* hexagonal SiC surfaces which exhibit a wealth of reconstructions. Many of these have been studied in great detail both from a fundamental as well as an applications point of view (for reviews, see Refs. 9–14). Very recently, Virojanadara *et al.*[15,16] added a particularly intriguing facet to the broad spectrum of SiC surface studies. They have shown that a C-terminated 4*H*-SiC(1$\bar{1}$02)-*c*(2×2) surface can be prepared by a diagonal cut through the SiC bulk unit cell and have investigated this surface by photoemission spectroscopy, scanning tunneling microscopy (STM), and low-energy electron diffraction (LEED). This type of SiC surfaces was first observed by Shiskin *et al.*[17] in an investigation of triangular channels in porous 4*H*-SiC, which was investigated later by Starke *et al.*[18] The 4*H*-SiC(1$\bar{1}$02)-*c*(2×2) surface resulting from the diagonal cut is largely free from defects, exhibiting basically an ideal stoichiometry and consists of a periodic arrangement of alternating cubic *and* hexagonal stripes with an atomic structure very close to the C-terminated cubic 3*C*-SiC(001) and hexagonal 6*H*-SiC(0001) surfaces, respectively. The very narrow (about 0.6 nm) alternating stripes constitute well-defined nanostructures which occur side by side on 4*H*-SiC(1$\bar{1}$02)-*c*(2×2). Based on their LEED, core-level spectroscopy (CLS), angle-resolved ultraviolet photoelectron spectroscopy (ARUPS), and STM data, the authors have suggested a model for the surface structure consisting of a specific distribution of Si adatoms on the hexagonal stripes in *H*3 sites with a particular arrangement of triple-bonded bridging carbon dimers on the cubic stripes. The authors emphasized that their tentative model should be viewed as a plausible starting point for a quantitative structure determination by crystallography or total-energy calculations.

To this end, we have investigated a whole variety of conceivable reconstruction models of 4*H*-SiC(1$\bar{1}$02)-*c*(2×2) by total-energy minimization calculations. Since the surface has cubic (001) and hexagonal (0001) stripes, we have scrutinized to which extent the known structural patterns of the 3*C*-SiC(001) and 6*H*-SiC(0001) surfaces can be carried over to the cubic and hexagonal stripes of 4*H*-SiC(1$\bar{1}$02)-*c*(2×2), respectively. Our results confirm the experimental assignment[16] of the adsorption sites of Si adatoms on the hexagonal stripes. As to the character and distribution of carbon dimers on the cubic stripes, however, our calculations reveal that alternative reconstruction models are more favorable than the one suggested by Virojanadara *et al.*[16] on the basis of their experimental data.

The paper is organized as follows. In Sec. II we briefly address the theoretical methods applied. In Sec. III we report our results and compare them with the experimental findings. Section III A presents the optimized surface structure for all models investigated. The electronic structure of the energetically most favorable reconstructions and that of the model suggested in Ref. 16 is presented in Sec. III B. Calculated

STM images are presented in Sec. III C and discussed in connection with experimental STM structure determinations. A brief summary concludes the paper in Sec. IV.

II. METHODOLOGY

Our calculations are carried out within the framework of the generalized gradient approximation (GGA) of density-functional theory. This approximation has been established as the method of choice for an appropriate description of the energetics involved in carbon dimerization, most prominently the difference between double- and triple-bonded carbon dimers. We use the exchange-correlation functional of Perdew and Wang[19] and nonlocal norm-conserving pseudopotentials[20] in separable form.[21] The wave functions are expanded employing a basis set of atom-centered Gaussian orbitals with several shells of s, p, d, and s^* symmetry per atom with appropriately determined decay constants.[22] The surface is treated within the supercell approach. Each slab consists of four Si-C double layers and is saturated by a layer of hydrogen atoms at the bottom. A vacuum layer of 10 Å separates neighboring slabs in order to avoid unphysical interactions between them. We employ the hybrid algorithm with Gaussian orbitals as basis sets and plane waves for the representation of the local part of the potential and the charge density as presented in Ref. 23. It makes use of Cartesian Gaussians and allows us to calculate matrix elements and charge densities in a very efficient way.[23] Brillouin-zone integrations are performed using a total set of 16 **k** points generated by the prescription of Monkhorst and Pack.[24] The positions of the atoms within the topmost five layers of each slab and the Si adatoms are allowed to relax until all components of the calculated Hellmann-Feynman and Pulay forces are smaller than 0.6 mRy/a_B. To overcome the well-known limitations of Kohn-Sham eigenvalues in describing the electronic structure, we include self-interaction corrections in the pseudopotentials yielding electronic band structures for SiC polytypes in very good agreement with experiment, as shown previously.[25] For example, the bulk band gap of 4H-SiC resulting as 3.30 eV from this approach is very close to the measured gap[1] of 3.26 eV.

To investigate the possibility of structural conversions between different conceivable reconstructions we determine respective minimum-energy pathways using the quadratic string (QS) method as presented by Burger and Yang in Ref. 26. The QS method is based on the same idea as the nudged elastic band method,[27] but it differs from the latter by integrating the perpendicular forces on the tangents of the reaction pathway numerically using a quadratic expansion of the potential-energy surface.[28]

STM images are calculated in the framework of the Tersoff-Hamann approach.[29] The constant-current operational mode is simulated by calculating topograms of constant charge density above the surface.

III. RESULTS

A. Atomic structure

We have investigated a large variety of conceivable $c(2\times2)$ reconstructions of the 4H-SiC$(1\bar{1}02)$ surface. For reference, we start out with the ideal surface which allows us to introduce some useful nomenclature easing the discussion of the rather complex surface reconstructions to follow.

1. Ideal surface and building blocks for reconstructions

Top and side views of the ideal C-terminated 4H-SiC$(1\bar{1}02)$ surface are shown in Fig. 1(a). Only the outermost Si-C double-layer is indicated. Carbon and Si atoms reside on the top and second layer, respectively.[30] Viewed along the $[\bar{1}101]$ direction, the surface consists of alternating stripes characteristic for the cubic 3C-SiC(001) and the hexagonal 6H-SiC(0001) surfaces. The respective stripes are separated by dashed lines in the top and side views and indicated by the labels c (for cubic) and h (for hexagonal) in the side view. The top view of the Si-C double layer shows hexagons within the hexagonal stripes. They are formed by three C and three Si atoms on the top and second layer, respectively. The top-layer C atoms are threefold coordinated to Si sublayer atoms. Consequently, they have only one dangling bond which is almost perpendicular to the surface. In the cubic stripes, the top-layer C atoms are twofold coordinated to Si sublayer atoms. They have two dangling bonds which lie in the $[\bar{1}\bar{1}20]$-$[1\bar{1}02]$ plane. The red dashed diamond indicated in Fig. 1(a) shows a $c(2\times2)$ unit cell which applies to the reconstructed surfaces to be discussed below. The ideal surface has twelve dangling bonds in the $c(2\times2)$ mesh (eight in the two cubic sections and four on the two hexagons). This is energetically very unfavorable so that the ideal surface reduces the number of its dangling bonds by an appropriate reconstruction. Both Si adatom adsorption and carbon dimerization are conceivable to this end because they can lead to a significant dangling-bond reduction.

As to the hexagonal stripes, it is well known from related reconstructions of the SiC$(000\bar{1})$ surface that adsorption of Si adatoms can lead to an efficient saturation of carbon dangling bonds.[31–33] A Si atom may adsorb in a *hollow* site above the center of a hexagon establishing three bonds to its carbon neighbors on the top layer ($H3$ site), or *on top* of a second-layer Si atom where it has four neighbors ($T4$ site)—the three C atoms on the top layer and the Si atom underneath on the second layer. Obviously, the ideal surface has two equivalent $H3$ and two equivalent $T4$ sites in the $c(2\times2)$ unit cell, which are marked by the positions H_1 and H_2 or T_1 and T_2, respectively, in Fig. 1(a).

Concerning the cubic stripes, it is likewise well known from related reconstructions of the C-terminated cubic SiC(001) surface that carbon dimerization reduces the number of dangling bonds significantly.[34–41] The most favorable atomic structure of this surface[35,36,40,41] turned out to be a staggered configuration of triple-bonded carbon dimers, each of which bridges two Si atoms on the second layer forming the so-called bridging-dimer (BD) model. This structure was found to be very close in total energy[37–41] to the so-called dimer row (DR) model, which features rows of double-bonded carbon dimers in its top layer. From the top view of Fig. 1(a) it is apparent that triple-bonded carbon dimers can form along the $[\bar{1}101]$ direction bridging two second-layer Si atoms. On the other hand, dimers can also form along the

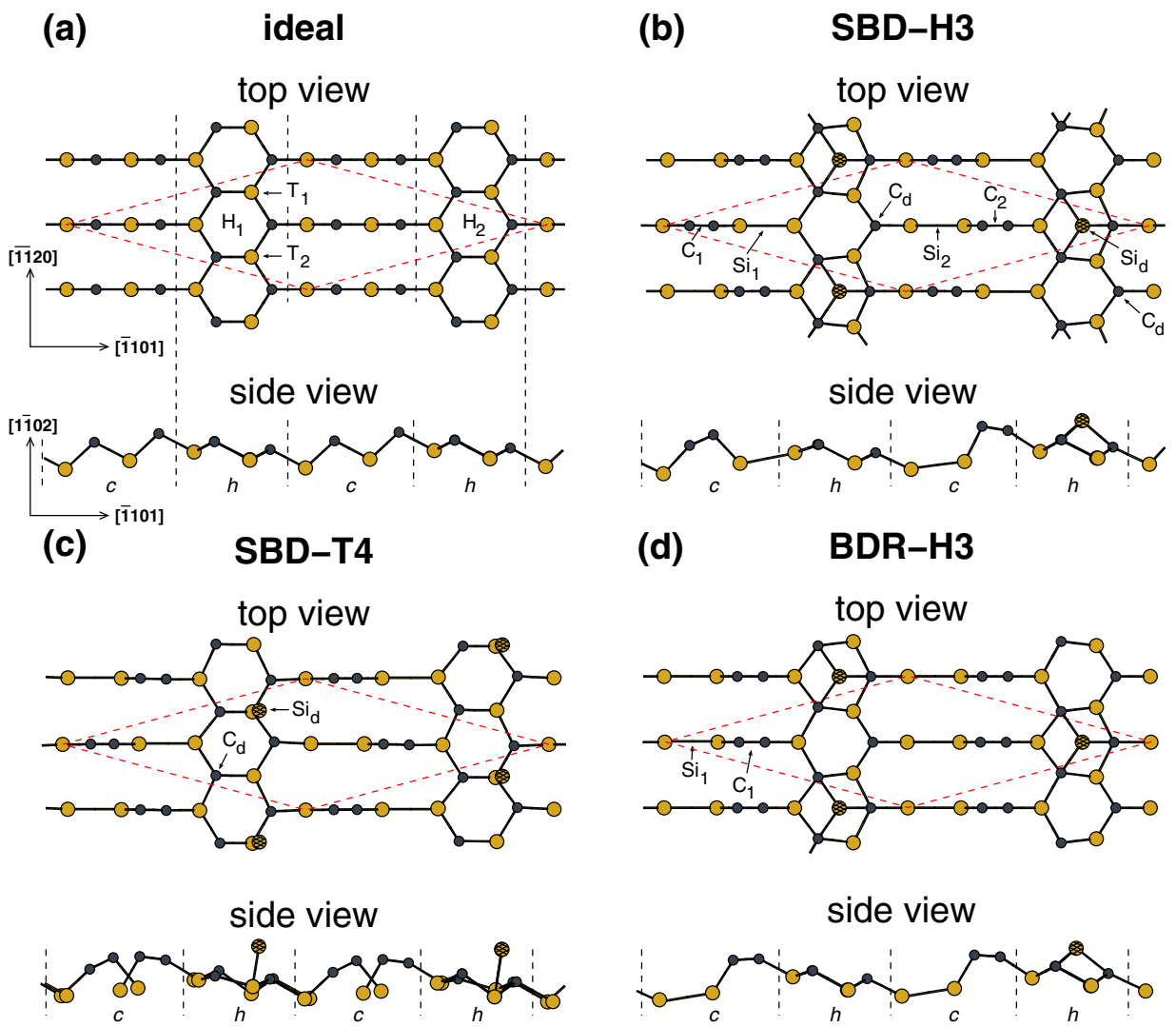

FIG. 1. (Color online) Top and side views of different reconstruction models of the 4*H*-SiC(1$\bar{1}$02)-$c(2\times2)$ surface: (a) ideal surface, [(b) and (c)] staggered bridging-dimer (SBD) model with the Si adatom in *H*3 or *T*4 position, respectively, as well as (d) bridging-dimer row (BDR) model with Si adatom in *H*3 position. Si and C surface atoms are represented by ochre (light gray) and black circles, respectively. The Si adatom is additionally marked by a crosshatching. The side views in (b) to (d) contain almost exclusively only the projected atoms from the unit cell. For the definition of the labels, see text. Note that all C-C dimers in (b)–(d) have triple bonds.

perpendicular [$\bar{1}\bar{1}$20] direction. In this case, they become double bonded since each carbon dimer atom is bound to two Si atoms on the second layer. Consequently, the different possibilities for separate reconstructions in the hexagonal and cubic stripes of the fairly large $c(2\times2)$ unit cell give rise to a large variety of conceivable structural models of the 4*H*-SiC(1$\bar{1}$02)-$c(2\times2)$ surface, which we address separately in the following.

2. Reconstructions with triple-bonded carbon dimers

First, we address bridging-dimer reconstruction models, one of which has been proposed by Virojanadara *et al.*[16] on the basis of their experimental data. On the basis of their core-level spectroscopy data the authors conclude that the surface composition is more or less stoichiometric. From an analysis of LEED intensities and STM images of 4*H*-SiC(1$\bar{1}$02)-$c(2\times2)$ in comparison with those of a nearly stoichiometric 6*H*-SiC(000$\bar{1}$)-(2×2) surface, the authors have inferred that a single Si adatom adsorbs in an *H*3 site above the center of one of the two hexagons in the unit cell. Concerning the cubic facets, they have assumed that a staggered pattern of bridging dimers closely related to the energetically favorable BD model of the cubic SiC(001)-$c(2\times2)$ surface exists on the 4*H*-SiC(1$\bar{1}$02)-$c(2\times2)$ surface as well. We have optimized the structure of this model by total-energy minimization. To this end, we have placed the Si adatom in an *H*3 site above the right hexagon (position H_2) in the unit cell. The resulting reconstruction model is shown by a top and a side view in Fig. 1(b). The Si adatom in the *H*3 site binds to the three subjacent C atoms in a tripod-like configuration fully saturating their dangling bonds. As a consequence, only one unsaturated dangling bond, which is basically perpendicular to the surface, remains on the Si ada-

tom. Correspondingly, we label the Si adatom as Si_d in Fig. 1(b). On the other hexagon in the unit cell only the dangling bond of the C atom that is not directly affected by Si adsorption [see Fig. 1(b)] remains unsaturated. It is also largely perpendicular to the surface. Therefore, we label this C atom as C_d in Fig. 1(b). In the following we will address the hexagon with an adsorbed Si atom as an *occupied* and that without a Si adatom as an *empty* hexagon. Note that by translational symmetry the Si_d and C_d atoms reside on neighboring hexagons of the structure [see Fig. 1(b)]. By this specific Si adsorption, the positions H_1 and H_2 at the ideal surface become inequivalent so that the reconstruction has $c(2\times2)$ symmetry.

On the cubic stripes there are two carbon dimers per unit cell [labeled C_1 and C_2 in Fig. 1(b)] bridging second-layer Si atoms. They are inequivalent due to their different positions in the unit cell. By symmetry, these dimers form a staggered bridging-dimer (SBD) structure. The respective full reconstruction with the Si adatom in an *H*3 site is referred to from now on as SBD-*H*3 model. The first carbon dimer C_1 is formed in the left half of the left while the second carbon dimer C_2 is formed in the right half of the right cubic stripe. We call this a l/r dimer configuration if necessary for clarity. Obviously, not only the l/r dimer configuration but also a r/l configuration (not shown in Fig. 1), as well as a r/r [see Fig. 1(d)] and a l/l configuration (not shown in Fig. 1) are compatible with the $c(2\times2)$ symmetry, constituting conceivable reconstructions of 4*H*-SiC$(1\bar{1}02)$-$c(2\times2)$ as well. The latter two structures feature bridging-dimer rows (BDR) along the $[\bar{1}\bar{1}20]$ direction and are, therefore, labeled BDR-*H*3 reconstructions. The appearance of two bridging carbon dimers per unit cell on the top layer of these four models is accompanied by the formation of two Si dimers on the second layer, which are indicated as Si_1 and Si_2 in Fig. 1(b). They have different distances to the filled and empty hexagons in the different models and their bonds are fully saturated. The triple-bonded bridging carbon dimers have no dangling bonds because three of the valence electrons of each involved C atom fill the C≡C dimer bonds, while the remaining valence electron establishes a bond to a Si atom on the second layer. As a consequence, there remain only two dangling bonds per $c(2\times2)$ unit cell, one on the surface carbon atom C_d and the other on the adatom Si_d. Thus, by these reconstructions the total number of dangling bonds is drastically reduced from twelve at the ideal to only two at the reconstructed surfaces, giving rise to a correspondingly large energy gain.

We now turn to respective reconstruction models with Si adatoms adsorbed in *T*4 sites. Figure 1(c) shows one such model resulting when we place the Si adatom in position T_1 [see Fig. 1(a)] and distribute the carbon dimers as in the SBD-*H*3 model in Fig. 1(b). Correspondingly, we labeled this model SBD-*T*4. The two possible positions T_1 and T_2 in Fig. 1(a) for *T*4 adsorption remain equivalent after forming bridging dimers in the cubic stripes since the mirror symmetry with respect to the central atomic line of the unit cell along the $[\bar{1}101]$ direction is preserved. Therefore, it is irrelevant whether we place the Si adatom in the T_1 or T_2 position. Note that the Si_d and C_d atoms now reside on the same hexagon. Actually, Fig. 1(c) shows the l/r SBD-*T*4 model. Apparently, also for *T*4 adsorption of Si, the three complementary models with r/l, r/r, and l/l distributions of the carbon dimers are compatible with the $c(2\times2)$ symmetry. The latter two models again feature bridging-dimer rows and are labeled BDR-*T*4 models, accordingly. We have, thus, specified eight unique reconstruction models, so far, which involve four different configurations of triple-bonded bridging carbon dimers on the cubic stripes and Si adatoms in either *H*3 or *T*4 sites on the hexagonal stripes of the surface.

In Table I, calculated bond lengths of carbon and Si dimers, as well as total energies of the different bridging-dimer models, are summarized. The latter are referred to the total energy of the l/r SBD-*H*3 model. The carbon dimer bond lengths in all four *H*3 models are near 1.23 Å, which is very close to respective bond lengths of triple-bonded carbon dimers in acetylene (C_2H_2) or in the BD model of SiC(001)-$c(2\times2)$ (see Table I). The Si dimers on the second layer adjust their bond lengths accordingly. Due to the existence of cubic and hexagonal sections in the large unit cell of 4*H*-SiC$(1\bar{1}02)$-$c(2\times2)$, the Si dimer bond lengths are larger at this surface than at the SiC(001)-$c(2\times2)$ surface (cf. Table I). Among the bridging-dimer *H*3 models the l/r SBD-*H*3 reconstruction, suggested previously,[16] turns out to be the least favorable. The other three dimer configurations lead to considerably lower total energies. The different distances of the top-layer carbon and second-layer Si dimers to the empty and occupied hexagons, on the one hand, as well as the different bond lengths of the second-layer Si dimers in the four models, on the other hand, account for the differences in total energy. For example, the l/r SBD-*H*3 structure exhibits the largest bond lengths of the Si dimers Si_1 and Si_2, rationalizing why this structure has the highest total energy. Respective results for the *T*4 models are given in Table I as well. In this case, the l/r and r/l configurations of the SBD model are equivalent by symmetry. Again, the staggered model (SBD-*T*4) has the highest total energy because it features the largest bond lengths of the Si dimers on the second layer as well. All *T*4 models have total energies that are considerably higher than those of the corresponding *H*3 models. The former are, thus, less favorable than the latter with the only exception of the r/r BDR-*T*4 model, which is lower in total energy by 0.3 eV than the l/r SBD-*H*3 model. Thus, it appears fairly unlikely that a bridging carbon dimer configuration combined with Si adatoms in *T*4 sites occurs at the 4*H*-SiC$(1\bar{1}02)$-$c(2\times2)$ surface. This conclusion is consistent with the experimental evidence.[16]

3. Reconstructions with double-bonded carbon dimers

In Sec. III A 2, we have considered triple-bonded bridging carbon dimers as building blocks for the reconstructions. However, double-bonded carbon dimers are comparably conceivable at 4*H*-SiC$(1\bar{1}02)$-$c(2\times2)$. The related BD and DR row reconstructions of SiC(001)-$c(2\times2)$ differ only slightly in total energy by some 0.1 eV,[40,41] which does not necessarily mean that triple-bonded carbon dimers are also more favorable at the much more complex 4*H*-SiC$(1\bar{1}02)$-$c(2\times2)$ surface. Therefore, we also consider reconstruction models

TABLE I. Dimer bond lengths (in Å) and total-energy differences per unit cell ΔE (in eV) of different reconstruction models of 4*H*-SiC($1\bar{1}02$)-$c(2\times2)$ referred to the energy of the l/r SBD-*H*3 model as resulting from our GGA calculations. Respective data for the bridging dimer and dimer row models of the cubic SiC(001) surface from Wang *et al.* (Ref. 41) are given for reference. In this case, ΔE is referred to the DR model. In addition, surface band gaps (in eV) as calculated using self-interaction-corrected (SIC) pseudopotentials are listed together with respective GGA band gaps. For further details, see text.

Model	BD configuration	d_{Si_1}	d_{Si_2}	d_{C_1}	d_{C_2}	ΔE	E_g^{SIC}	E_g^{GGA}
Reconstructions with triple-bonded staggered bridging dimers (SBD) or bridging-dimer rows (BDR)								
SBD-*H*3	l/r	2.61	2.57	1.23	1.24	0.00	1.34	0.14
SBD-*H*3	r/l	2.55	2.51	1.23	1.24	−0.64	1.29	0.46
BDR-*H*3	l/l	2.47	2.37	1.22	1.23	−0.61	1.65	0.36
BDR-*H*3	r/r	2.48	2.46	1.22	1.22	−0.81	1.37	0.20
SBD-*T*4	l/r	2.60	2.56	1.23	1.23	0.25	1.49	0.06
SBD-*T*4	r/l	2.60	2.56	1.23	1.23	0.25	1.49	0.06
BDR-*T*4	l/l	2.44	2.44	1.22	1.22	−0.01	1.52	0.09
BDR-*T*4	r/r	2.48	2.48	1.22	1.22	−0.30	1.19	0.02
Reconstructions with double-bonded staggered dimers (SD) or dimer pairs (DP)								
SD-*H*3				1.38	1.38	−1.73	1.53	0.28
DP-*H*3				1.38	1.38	−2.08	1.49	0.26
SD-$T4_1$				1.38	1.39	−0.75	1.42	Metallic
DP-$T4_1$				1.38	1.37	−1.74	1.29	Metallic
SD-$T4_2$				1.38	1.38	−1.50	1.37	0.04
DP-$T4_2$				1.38	1.38	−1.23	1.42	0.02
Bridging-dimer (BD) or dimer row (DR) reconstructions of 3*C*-SiC(001)								
BD $c(2\times2)$		2.42		1.23		−0.11	2.46	1.24
DR $p(2\times1)$				1.39		0.00	0.99	Metallic

featuring double-bonded carbon dimers. From Fig. 1(a) it is obvious that neighboring twofold coordinated surface C atoms can easily tilt along the $[\bar{1}\bar{1}20]$ direction toward each other until their free dangling bonds establish a dimer bond. Neither bond breaking nor bond-length changes are involved. The resulting C=C dimers can again arrange in staggered or row configurations.

Figure 2 shows top views of three exemplary reconstructions involving double-bonded carbon dimers. In Fig. 2(a) the carbon dimers form staggered-dimer (SD) patterns and the Si adatoms occupy *H*3 sites (SD-*H*3). The reconstruction shown in Fig. 2(b) features dimer pairs (DP) with the Si adatom in the same *H*3 site, as before (DP-*H*3). In both of these models there are two possible configurations of the dimers in the two halves of the unit cell but they are equivalent by symmetry. So there are only two unique *H*3 structures. The double-bonded carbon dimers are symmetric and there are no Si dimers on the second layer of these structures. The formation of double-bonded dimers does not conserve the mirror symmetry of the ideal surface mentioned above. Consequently, the positions T_1 and T_2 [see Fig. 1(a)] for Si adatom adsorption in a *T*4 site are no longer equivalent. Thus, we have to differentiate between models with Si adatoms adsorbed in a T_1 or a T_2 position, respectively, which we label $T4_1$ [as shown in Fig. 2(c)] or $T4_2$ models, accordingly. Also in both of these cases, there are only two unique structures (SD and DP) by symmetry.

The carbon dimer bond lengths and total energies of the respective six reconstruction models are also listed in Table I. The bond lengths of the carbon dimers in all models result basically as 1.38 Å as is typical for C=C double bonds well known from ethane (C_2H_4) or the related DR model of the SiC(001)-$p(2\times1)$ surface (cf. Table I). Energetically, both the SD-*H*3 and DP-*H*3 models turn out to be substantially more favorable than any of the bridging-dimer models discussed above. Their energy differences with respect to the l/r SBD-*H*3 model amount to about 1.73 (SD-*H*3) and 2.08 eV (DP-*H*3), respectively. The difference in total energy of 0.35 eV between these two models originates from different relaxations in the subsurface layers. The respective *T*4 models are again all higher in total energy than their *H*3 counterparts. Nevertheless, most of them have total energies that are more than 1 eV lower than those of the respective SBD-*T*4 and BDR-*T*4 models, discussed in Sec. III A 2.

Thus, most of the reconstruction models with double-bonded carbon dimers turn out to be more favorable than those involving triple-bonded bridging carbon dimers in the cubic stripes of the surface. Double-bonded carbon dimers can easily form without bond breaking or bond-length changes, as described above. The formation of triple-bonded bridging carbon dimers, on the contrary, necessitates break-

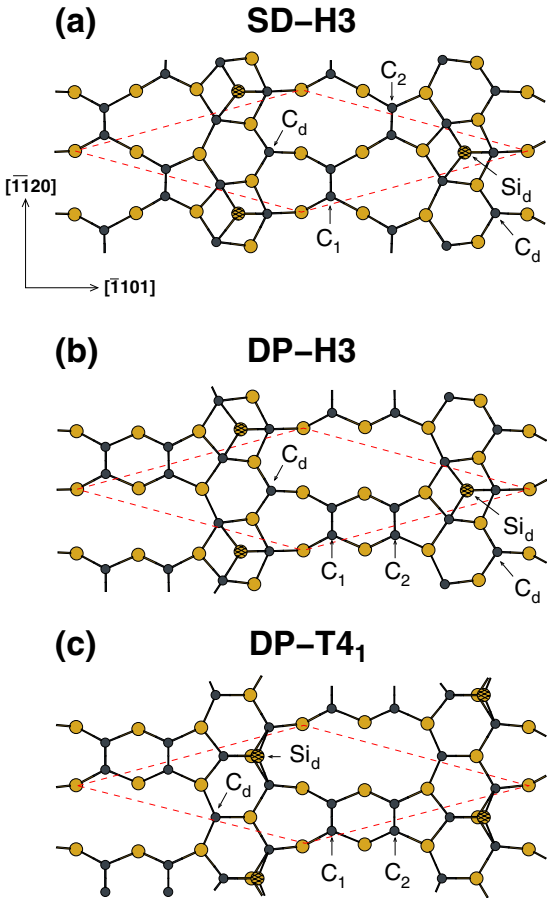

FIG. 2. (Color online) Top views of different reconstruction models of the 4*H*-SiC(1$\bar{1}$02)-$c(2\times2)$ surface: (a) staggered-dimer (SD) and (b) dimer-pair (DP) models with the Si adatom in *H*3 position, (c) dimer-pair (DP) model with the Si adatom in $T4_1$ position. For further details, see text and caption of Fig. 1. Note that all C-C dimers in this figure have double bonds.

ing three Si–C bonds and forming three new bonds (one carbon dimer bond at the surface, one Si dimer bond on the second layer, and one Si–C bond between the top and second layer). As a consequence, a very delicate balance between the energy loss and gain involved in breaking three original and forming three new bonds, respectively, determines which reconstruction mechanism is more favorable. At the SiC(001) surface, the balance is slightly in favor of the triple-bonded bridging dimers because of the highly symmetric environment both perpendicular and parallel to the surface. In contrast, the 4*H*-SiC(1$\bar{1}$02)-$c(2\times2)$ surface is not only different because it exhibits alternating cubic and hexagonal stripes parallel to the surface, but also because it has a considerably more complex structure perpendicular to the surface. This much more complex environment and the intricate interactions between the atoms on the respective stripes and in the surface layers result in a different energetic order of configurations with triple-bonded bridging versus double-bonded carbon dimers on 4*H*-SiC(1$\bar{1}$02)-$c(2\times2)$ than on the purely cubic SiC(001) surface.

On the basis of our structure optimization results for the 14 considered reconstruction models, we conclude that the

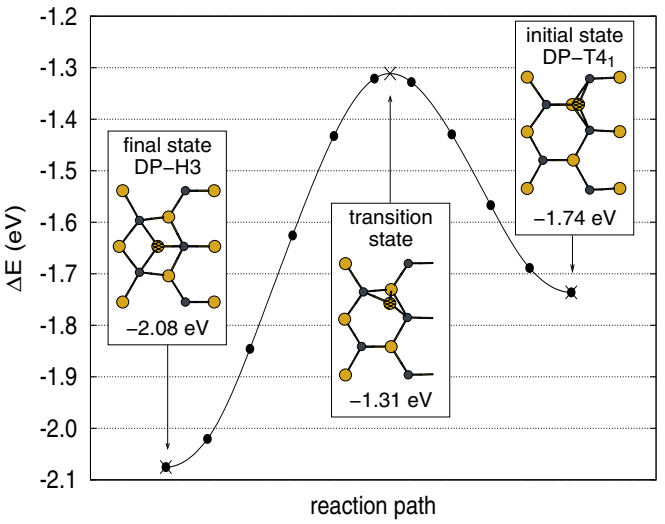

FIG. 3. (Color online) Minimum energy pathway (in eV) for the conversion from the initial DP-$T4_1$ to the final DP-*H*3 structure of the 4*H*-SiC(1$\bar{1}$02)-$c(2\times2)$ surface. The insets show top views of the surface atomic structure around the occupied hexagon. For details, see text.

DP-*H*3 model constitutes the most favorable reconstruction of the 4*H*-SiC(1$\bar{1}$02)-$c(2\times2)$ surface. Virojanadara *et al.*[16] reported C 1*s* and Si 2*p* core-level spectra of the surface. They observed one shifted component in the C 1*s* and two shifted components in the Si 2*p* spectra, respectively. These surface-induced shifts were interpreted in terms of the configuration of surface features in the SBD-*H*3 model. The same reasoning would apply to the DP-*H*3 model so that we cannot identify any model-discerning features from a comparison with the core-level spectra.

Let us finally address a more subtle point concerning the surface reconstruction. From a purely thermodynamics point of view the DP-*H*3 model is the most favorable reconstruction. Yet, it is conceivable that under experimental surface preparation conditions,[16] the Si adatoms might adsorb in metastable *T*4 sites. The question then arises whether the *T*4 reconstructions are thermodynamically stable or whether they convert from a metastable *T*4 to the more stable *H*3 structure. To address this question, we have calculated minimum-energy pathways (MEP) for this type of conversion. As an example, Fig. 3 shows the MEP from the DP-$T4_1$ to the DP-*H*3 reconstruction. The local atomic structure around the occupied hexagon is shown in the insets for the initial, transition, and final states. Initially, the adatom moves from the $T4_1$ toward the *H*3 position stretching its bond to the upper C atom (cf. Fig. 3) and compressing its bonds to the other two C atoms. This process obviously involves a steady energy loss. When the Si atom has arrived in the transition state, its bond to the upper C atom has become broken. Moving further to the final state, the adatom continuously gains energy until it eventually occupies the *H*3 site. In the final state it forms three covalent bonds with the three subjacent C atoms. Obviously, there is an energy barrier of about 0.4 eV that needs to be overcome by the Si adatom on its MEP from the $T4_1$ to the *H*3 site. We find similar barrier energies for respective $T4 \leftrightarrow H3$ conversions of other recon-

struction models addressed in this work. In view of the fact that Si adatoms that may adsorb initially in local minimum $T4$ sites have sufficient time and energy at high surface preparation temperature to surmount a barrier of 0.4 eV, we consider it unlikely that Si adatoms are observed in $T4$ sites when the surface is eventually investigated at room temperature. We note in passing that we have also studied structural conversions from models with double-bonded dimers to models with triple-bonded bridging dimers. For example, for the conversion from the SD-$H3$ to the l/r SBD-$H3$ model, we find a barrier of some 1.9 eV, corroborating that a large energy is involved in creating bridging dimers in the cubic stripes of the 4H-SiC($1\bar{1}02$)-$c(2\times2)$ surface.

B. Electronic structure

We have investigated the electronic properties of all reconstruction models optimized in Sec. III A employing self-interaction-corrected pseudopotentials, as described in the Appendix. For short, we only present and discuss the surface band structures of the energetically most favorable DP-$H3$ and DP-$T4_1$ models, as well as the l/r SBD-$H3$ model proposed by Virojanadara *et al.*[16] Figure 4(a) shows the surface Brillouin zone (SBZ) and the respective surface band structures resulting from our self-interaction-correction calculations plotted in (b) to (d) within an energy range near the fundamental gap from −3 to 5 eV. The gray shaded areas in the band-structure plots indicate the projected bulk band structure of 4H-SiC. Based on a Mulliken analysis, we have marked bands originating from Si or C surface dangling bonds by ochre (light gray) and black triangles, respectively. Bands originating from the Si dimers Si_1 and Si_2 on the second layer of the SBD-$H3$ model are denoted by open and full ochre (light gray) circles in (d), while bands originating from the top-layer carbon dimers C_1 and C_2 are indicated by open and full black circles in (b) to (d), respectively. We refrain from showing the full band structures since the available photoemission data are limited to the gap energy region.[16] We only note in passing that all three band structures exhibit weakly dispersing C 2s surface bands near the lower edge of the projected carbon bulk bands around −15 eV and weakly dispersing p-type surface bands within the ionic gap around −10 eV. The fundamental band gaps of all reconstructions investigated are given in Table I.

The carbon dimers of the DP-$H3$ model give rise to bonding ($C_{1,2}$) and antibonding ($C^*_{1,2}$) bands close to the upper and lower edges of the projected valence and conduction bands, respectively [see Fig. 4(b)]. The dangling bonds on the C_d and Si_d surface atoms yield dangling-bond bands, which we also label C_d and Si_d for simplicity. These bands show only weak dispersions due to the weak interaction of the respective dangling bonds. The C_d band is occupied while the Si_d band is empty. Charge-density contours of respective surface states at the Y' point of the SBZ, shown in Figs. 5(a)–5(d), confirm the above assignments. The main contribution to the Si_d state originates form the empty dangling bond at the Si adatom in $H3$ position [see Fig. 5(a)] but there are also contributions at the three subjacent C atoms (only one lies in the drawing plane). The dominant contribution to the C_d state apparently comes from the occupied dangling bond at the C_d surface atom [see Fig. 5(b)]. The charge density in Fig. 5(c) clearly exhibits the bonding character of the C_1 state, while the charge density in Fig. 5(d) shows a nodal plane between the two C atoms of the C_1 dimer confirming the antibonding character of the C^*_1 state.

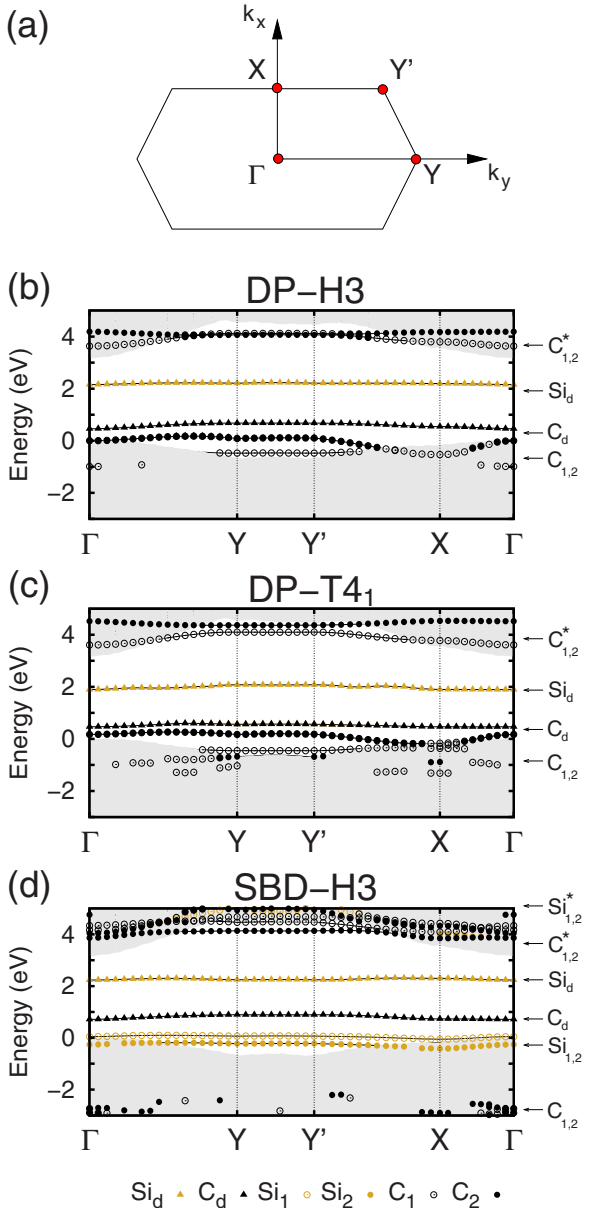

FIG. 4. (Color online) Surface Brillouin zone (a) and sections of the band structures of the DP-$H3$ (b), DP-$T4_1$ (c) and the l/r SBD-$H3$ (d) models, as resulting from our SIC calculations. Bands that can uniquely be assigned to Si or C atoms are marked by ochre (light gray) and black symbols. Triangles represent bands originating from surface atoms featuring dangling bonds while open and filled circles represent bands originating from Si and carbon dimers.

The DP-$T4_1$ model exhibits largely similar surface bands [see Fig. 4(c)]. Those originating from the bonding and antibonding states of the carbon dimers are only slightly affected by the change in the Si adsorption site from $H3$ to $T4_1$. Only the splitting of the $C^*_{1,2}$ dimer bands is somewhat

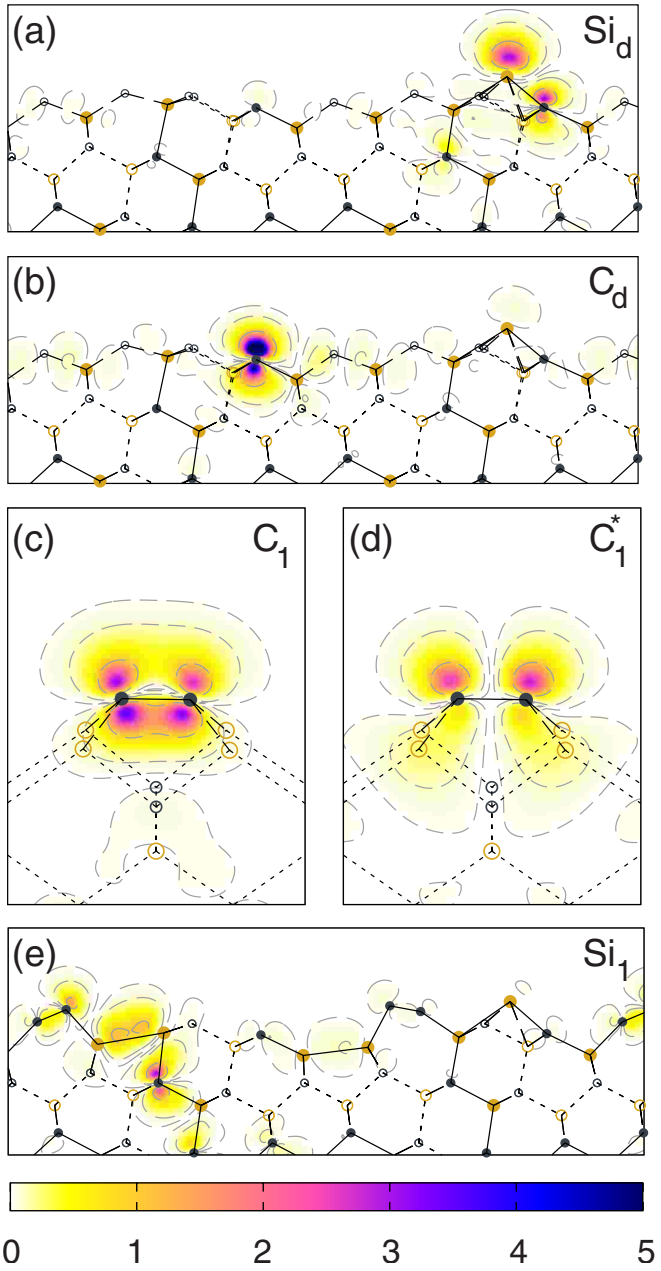

FIG. 5. (Color online) Charge-density contours (in $10^{-2}a_B^{-3}$) of the Si_d, C_d, C_1, C_1^*, and Si_1 states at the Y' point of the SBZ. Si and C atoms are depicted by ochre (light gray) and black dots, respectively. Filled (open) symbols represent atoms within (outside) the drawing plane. Panels (a) to (d) show charge densities of the DP-*H*3 model of 4*H*-SiC($1\bar{1}02$)-$c(2\times2)$ surface while (e) shows one charge density of the SBD-*H*3 model. Panels (a), (b), and (e) are plotted in the $[\bar{1}101]$-$[1\bar{1}02]$ plane while panels (c) and (d) are plotted in the $[\bar{1}\bar{1}20]$-$[1\bar{1}02]$ plane containing the carbon dimer C_1.

larger than in the DP-*H*3 band structure, which appears to be due to the structural differences in the hexagonal stripes of the DP-$T4_1$, as compared to the DP-*H*3 model [cf. Figs. 2(b) and 2(c)]. The charge densities of respective states are very similar to those of the DP-*H*3 model. We, therefore, refrain from showing any of them for shortness sake.

The band structure of the SBD-*H*3 model in Fig. 4(d) shows two characteristic differences to the former band structures. On one hand, the bonding and antibonding bands originating from the triple-bonded C≡C dimers occur lower and higher in energy, respectively, than in the DP models whose C=C bonds are comparatively weaker. In addition, the SBD-*H*3 model features Si dimers on the second layer (not occurring in the DP models), which give rise to two bonding dimer bands indicated as $Si_{1,2}$ residing slightly above the projected bulk valence bands and two antibonding dimer bands indicated as $Si_{1,2}^*$, which are close in energy to the antibonding bands of the carbon dimers. The charge density in Fig. 5(e) confirms this assignment, showing that a large contribution to the Si_1 state originates from the Si_1 dimer. In addition, admixtures from the neighboring C atom on the next subsurface layer, as well as from the C_1 dimer at the top layer contribute to this state.

The ARUPS data presented in Ref. 16 exhibit a band gap of at least 1 eV and four occupied bands (labeled S1-S4), which were tentatively interpreted as resulting from surface states or surface resonances since they were found to be more sensitive to surface contamination than other measured valence-band features. Only the band S1, which occurs highest in energy, could clearly be identified as a surface-state band since it appears in the projected bulk band gap. It has a very weak dispersion of 0.1 ± 0.05 eV only. The other three bands show more pronounced dispersions in sections of the SBZ. For example, the band S2, observed 0.7 eV below the S1 band at Γ, exhibits a dispersion of 0.55 eV from the *Y* to the *X* point. It was assigned to the Si adatoms on the hexagonal stripes. Since the valence-band maximum (E_{VBM}) could not be identified in experiment, the bands S2-S4 could not definitely be attributed to particular surface states or resonances. Our surface band structures are referred to E_{VBM}. Therefore, we cannot directly compare them with the ARUPS data on an absolute energy scale. Nevertheless, it appears fairly clear that the band S1 observed in experiment originates from the weakly dispersing occupied carbon dangling-bond band C_d, resulting in all three band structures [see Figs. 4(b)–4(d)]. Likewise, all three calculated band structures show surface band gaps larger than 1 eV (cf. Table I), which is consistent with the experimentally determined gap as well. The interpretation of the S2 band suggested in Ref. 16 as resulting from the Si adatoms on the hexagonal stripes, contradicts our results in that the dangling bonds on the Si adatoms are empty, as noted above. There are, however, groups of occupied bands ($C_{1,2}$ or $Si_{1,2}$, respectively) below the C_d band in the band structures of the DP-*H*3 and SBD-*H*3 models [see Figs. 4(b) and 4(d)], which could be related to the measured S2 band. The $C_{1,2}$ bands in the band structure of the DP-*H*3 model in fact occur only about 0.5 eV below the C_d band at Γ, but their dispersion of 0.55 eV is in excellent agreement with experiment. The $Si_{1,2}$ bands of the SBD-*H*3 model indeed occur 0.7 eV below the respective C_d band, which would be in agreement with experiment, but they actually show only a very weak dispersion in contradiction to experiment. As to the measured bands S3 and S4, there are no direct counterparts in the calculated band structures [see Figs. 4(b)–4(d)]. We have scrutinized the energy range from 0 to −3 eV, looking for pronounced surface reso-

nances but we could not identify any. This discrepancy could be related to bulk states with a small $k_\perp$ dispersion giving rise to uncertainties in the band mapping carried out in experiment.[16] To this end we have calculated the bulk band structure of 4*H*-SiC for $k_\perp$ along the surface normal. As a matter of fact, we find two groups of rather flat bulk bands in the energy region in question.

In general, our calculations yield band gaps for all 14 presented models of the 4*H*-SiC$(1\bar{1}02)$-$c(2\times2)$ surface in the range of 1.19 to 1.65 eV (cf. Table I). They are fairly similar due to the similar nature of the states forming the gap and all of them are consistent with the gap estimated from photoemission.[16] This corroborates that band gaps alone are not suitable to discern between different reconstruction models by comparison with experiment for the surface at hand.

C. Scanning tunneling microscopy

From the discussion of the band structures of different reconstruction models in Sec. III B, it has become quite evident that a comparison of the calculated surface band structures with the ARUPS data[16] is not sufficiently instructive to unequivocally conclude which model has actually been observed in experiment. However, the band structures of the DP-*H*3 and SBD-*H*3 models in Figs. 4(b) and 4(d) reveal that it is possible to identify other features that might be useful to resolve this question. The carbon dimers giving rise to the antibonding bands $C^*_{1,2}$, residing within the projected bulk band-gap region as true surface-state bands, are oriented orthogonally in the DP and SBD models, respectively. In addition, the antibonding Si dimer bands $Si^*_{1,2}$ occur in the same energy region as the $C^*_{1,2}$ bands of the SBD model. It is to be expected, therefore, that empty-state STM images at bias voltages corresponding to that particular energy region show characteristic differences for the two models.

In Figs. 6 and 7 we show calculated constant-current STM images for specifically chosen empty states of the SBD-*H*3 and DP-*H*3 models. The images in the upper (lower) panels were calculated for a bias voltage of 1.5 V (3.7 V) above the highest occupied surface state with an energy window of ±0.25 eV. At a bias voltage of 1.5 V, only states of the empty Si_d band, which is present in both surface models at the same energy, can contribute to the images. As a consequence, the STM images in the top panels of Figs. 6 and 7 which only sample the hexagonal stripes are largely similar. The bright protrusions originate from the empty dangling bonds on the Si adatoms in *H*3 sites and their almost triangular shape arises from the charge-density contributions of the antibonding states of the Si–C bonds to the three subjacent C atoms, as discussed above [cf. Fig. 5(a)]. Obviously, the spatial arrangement of the protrusions exhibits the $c(2\times2)$ symmetry of the surface. An arrangement of similar protrusions is seen in experiment as well.[16] This finding corroborates that the dangling bonds at the Si adatoms are empty, indeed, rather than occupied, as conjectured in the interpretation of the ARUPS data[16] (cf. Sec. III B). Likewise, the vertical and horizontal distances of the bright protrusions results as 6.22 and 11.51 Å from our calculations in good

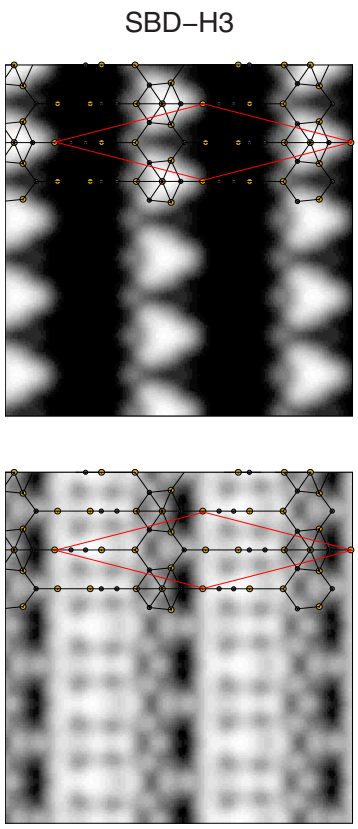

FIG. 6. (Color online) Calculated constant-current STM images for empty states of the SBD-*H*3 model of the 4*H*-SiC$(1\bar{1}02)$-$c(2\times2)$ surface. The upper and lower panels show images calculated at bias voltages of 1.5 and 3.7 V, respectively, with an energy window of ±0.25 eV in both cases. One exemplary surface unit cell with the respective atoms is superimposed on both images.

accord with the experimentally determined distances of 6.16 and 11.42 Å, respectively, given the fact that GGA overestimates lattice constants by about 1%. The above results yield only information on the distribution of the Si adatoms on the hexagonal stripes since only states of the empty Si_d band are sampled.

To become more sensitive to the different dimers and their different arrangement on the cubic stripes of the SBD and DP models, we have calculated STM images for a more appropriate range of the bias voltage. Respective STM images simulated again with an energy window of ±0.25 eV, but now at a bias voltage of 3.7 V are shown in the lower panels of Figs. 6 and 7. In this energy range the previously mentioned antibonding carbon dimer states $C^*_{1,2}$ are accessible for both reconstructions. Their nature and origin is very different in the two models, as discussed in detail in Secs. III A and III B. As a consequence, entirely different STM images result now sampling the cubic stripes of the surface. Very amazingly, at a first glance, the STM image for the SBD model shows straight rows of somewhat intricate protrusions along the $[\bar{1}\bar{1}20]$ direction, pretending a 2×2 reconstruction, although the carbon dimers are arranged in a staggered pattern. This is due to the fact that not only the antibonding carbon dimer states $C^*_{1,2}$ but also the antibonding Si dimer states $Si^*_{1,2}$ on the second layer [see Fig. 4(d)] contribute to

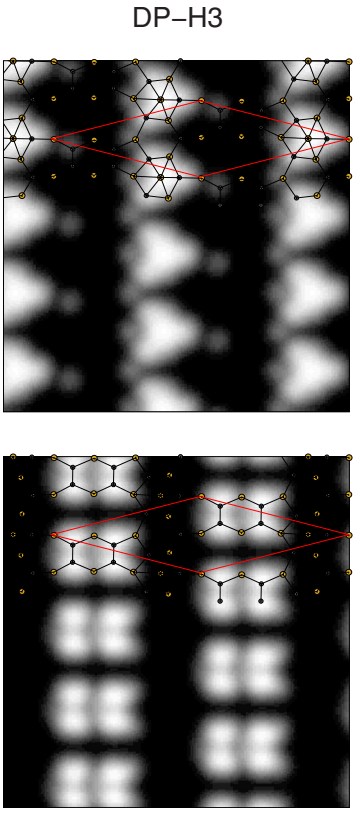

FIG. 7. (Color online) Calculated constant-current STM images for empty states at the DP-$H3$ model of the $4H$-SiC$(1\bar{1}02)$-$c(2\times2)$ surface. The upper and lower panels show images calculated at bias voltages of 1.5 and 3.7 V, respectively. For further details, see caption of Fig. 6.

this image. Thus, if $4H$-SiC$(1\bar{1}02)$-$c(2\times2)$ reconstructs in the SBD-$H3$ model, an experimental confirmation of the full structure by STM from the subtle intensity variations originating from the antibonding carbon and Si dimer states, respectively, could be very difficult.

In contrast, the respective STM image of the DP-$H3$ model calculated at 3.7 V turns out to be much more clear cut. From the lack of Si dimers in this model it follows that the image only contains contributions from the antibonding $C^*_{1,2}$ states of the C=C dimers. As a consequence, the simulated image in the lower panel of Fig. 7 clearly reveals the pair configuration of the double-bonded carbon dimers at the $4H$-SiC$(1\bar{1}02)$-$c(2\times2)$ surface. The dimer pairs occur at different heights in the left and right cubic stripes, as discussed in Sec. III A. The nodal plane in the middle of the individual dimer bonds is clearly revealed as was the case in the side view of the charge density in Fig. 5(d). Note that the STM image is plotted in a plane orthogonal to the plotting plane of the charge density. The dimer pair arrangement in the DP-$H3$ model, thus, gives rise to very localized signals in the calculated STM image.

Given these substantial differences of empty-state STM images in the SBD-$H3$ and DP-$H3$ models, experimental images taken at respectively large bias voltages should yield a clear indication of the type of carbon dimers forming on the $4H$-SiC$(1\bar{1}02)$-$c(2\times2)$ surface and their spatial arrangement, thus, allowing for an identification of the surface structure not only in the hexagonal but also in the cubic stripes.

IV. SUMMARY

The surface atomic and electronic structure of 14 distinctly different reconstruction models of the $4H$-SiC$(1\bar{1}02)$-$c(2\times2)$ surface has been investigated by *ab initio* GGA and self-interaction-correction calculations, respectively. Si adatom adsorption on the hexagonal stripes of the surface in $H3$ and $T4$ positions, as well as a number of configurations of triple-bonded bridging C≡C dimers or double-bonded C=C dimers on the cubic stripes, has been considered. All reconstruction models investigated exhibit only two surface dangling bonds while the ideal surface has twelve dangling bonds per unit cell. The DP-$H3$ reconstruction model featuring Si adatoms in $H3$ sites on the hexagonal stripes and pairs of double-bonded carbon dimers on the cubic stripes is found to be energetically most favorable. Our results suggest that Si adatoms which might conceivably adsorb initially in metastable $T4$ sites convert to the most stable $H3$ sites during experimental preparation of the surface at high temperature. Therefore, it is not to be expected that Si adatoms are found in $T4$ sites when the surface is eventually investigated at room temperature. The surface electronic structure of the two energetically most favorable reconstructions (DP-$H3$ and DP-$T4_1$) and that of the previously suggested staggered bridging-dimer model with Si adatoms in $H3$ sites (SBD-$H3$) has been discussed in comparison with ARUPS data. So far, this comparison showing several good agreements but also some disagreements between theory and experiment is not yet sufficiently revealing to allow for an identification of the true reconstruction of $4H$-SiC$(1\bar{1}02)$-$c(2\times2)$. Finally STM images have been reported which reveal that particular empty-state STM topograms could resolve the question when the bias voltage is chosen appropriately. Nevertheless, a decisive structure identification by comparing theory with the available experimental data is not yet possible, at present. This situation calls for a joint experimental (LEED, STM, CLS, and ARUPS) and theoretical (total energy, band structure, charge densities, and STM images) investigation, which would try to narrow down the number of possible structures to a very few and then investigate these candidates in great detail by as broad a spectrum of methods as possible.

ACKNOWLEDGMENTS

We would like to thank U. Starke for useful discussions and helpful comments on the manuscript. The total-energy minimization calculations were carried out on the computers of the Morfeus-GRID at the Westfälische Wilhelms-Universität Münster using CONDOR (see Ref. 42).

APPENDIX

While the atomic structure of bulk semiconductors and their surfaces can be calculated with a good level of confidence within GGA, the respective electronic structure result-

ing within this approximation suffers from the well-known band-gap underestimate. For 4*H*-SiC, e. g., the GGA bulk band gap of 2.26 eV is some 30% smaller than the experimental gap[1] of 3.26 eV. This deficiency can largely be attributed to unphysical self-interactions inherent in GGA or local-density approximation calculations,[43] leading to an overestimation of the energetic position of occupied bands. To overcome this problem we employ self-interaction-corrected (SIC) pseudopotentials, which yield basically the same atomic but a much improved electronic structure, as described in detail, e.g., in Ref. 25. Using this approach, we have determined among others the bulk electronic structure of four SiC polytypes and have found them to be in excellent agreement with experiment. It should be noted that the SIC pseudopotentials have only a small and implicit influence on conduction bands while they lead to significant downward shifts of valence bands. This physical effect is obscured in SIC band structures when they are referred to E_{VBM} as usual. In that case, the band structures appear to show that the conduction bands have shifted to higher energies with respect to the valence bands. Actually, however, the valence bands have shifted to lower energies with respect to the conduction bands.

With this fact in mind, we now briefly address a methodological aspect concerning our electronic structure calculations for the 4*H*-SiC$(1\bar{1}02)$-$c(2\times2)$ surface. In our approach, *atomic* SIC corrections to the standard pseudopotentials are determined and transferred to the solid by a well-defined procedure.[25] They predominantly affect the energetic positions of occupied bands, i.e., the C 2*s*, C 2*p*, and Si 3*s* valence bands in bulk silicon carbide. Chemically reactive surfaces such as 4*H*-SiC$(1\bar{1}02)$-$c(2\times2)$ typically possess salient surface states whose character deviates significantly from that of bulk states. For instance, dimer formation leads to bonding and antibonding dimer states as in the case of the C_1 and C_1^* states shown in Figs. 5(c) and 5(d), which originate mainly from C 2*p* states. In view of this fact, it becomes immediately apparent that an atomic self-interaction correction of C 2*p* states similarly affects the occupied bonding (C_1) as well as the empty antibonding band (C_1^*). Consequently, in a straightforward SIC calculation empty surface states would experience the same self-interaction correction as occupied surface states. This is unphysical since empty states are not subject to self-interactions. This inadequacy needs to be accounted for in surface electronic structure calculations. The effect can be quantified for each band n and $\mathbf{k}$ point by calculating the expectation value of the nonlocal SIC operator containing the approximate self-interaction corrections as defined in Eq. (13) of Ref. 25,

$$\Delta\epsilon_{n,\mathbf{k}}^{\mathrm{SIC}} = \langle\psi_{n,\mathbf{k}}|\hat{V}_{\mathrm{nloc}}^{\mathrm{SIC}}|\psi_{n,\mathbf{k}}\rangle \leq 0. \tag{A1}$$

When n_{occ} is the number of occupied bands, $\Delta\epsilon_{n,\mathbf{k}}^{\mathrm{SIC}}$ should vanish for all bands $n > n_{\mathrm{occ}}$. One way to eliminate the spurious self-interaction correction of empty surface states is to subtract the respective correction as given in Eq. (A1) from the calculated single-particle energies $\epsilon_{n,\mathbf{k}}^{\mathrm{SIC}}$ for unoccupied bands and plot the band structure according to

$$\tilde{\epsilon}_{n,\mathbf{k}}^{\mathrm{SIC}} = \begin{cases} \epsilon_{n,\mathbf{k}}^{\mathrm{SIC}} & \text{for } n \leq n_{\mathrm{occ}} \\ \epsilon_{n,\mathbf{k}}^{\mathrm{SIC}} - \Delta\epsilon_{n,\mathbf{k}}^{\mathrm{SIC}} & \text{for } n > n_{\mathrm{occ}}. \end{cases} \tag{A2}$$

We emphasize at this point that this elimination of spurious self-interaction corrections of empty surface states employing Eq. (A2) does not change the bulk band structures as calculated by the standard approach[25] by more than a couple of meV.

In order to evaluate the quality of the SIC method described above, we have also applied it to the surface electronic structure of the 3*C*-SiC(001) surface in both the $c(2\times2)$ bridging dimer and the 2×1 dimer row models. Our results are in very good agreement with angle-resolved (inverse) photoelectron spectroscopy data[36,44] for the BD model and with elaborate quasiparticle calculations[39] for the DR model. We find a gap of 0.99 eV for the DR model (cf. Table I) which is close to the gap of 0.94 eV resulting from the quasiparticle calculations.[39] We infer from these agreements that the band structures for the models of the 4*H*-SiC$(1\bar{1}02)$-$c(2\times2)$ surface, as calculated using the SIC approach in this work, are also reliable.

*baumeier@uni-muenster.de

[1] *Properties of Silicon Carbide*, EMIS Datareviews Series Vol. 13, edited by G. L. Harris (INSPEC, London, 1995).
[2] S. E. Saddow and A. Agrawal, *Advances in Silicon Carbide Processing and Applications* (Artech House, Boston-London, 2004).
[3] *Silicon Carbide: Recent Major Advances*, edited by W. J. Choyke, H. M. Matsunami, and G. Pensl (Springer, Berlin, 2004).
[4] M. A. Capano and R. J. Trew, MRS Bull. **22**, 19 (1997).
[5] *Silicon Carbide: A Review of Fundamental Questions and Applications to Current Device Technology*, edited by W. J. Choyke, H. M. Matsunami, and G. Pensl (Akademie, Berlin, 1998), Vols. 1 and 2.
[6] K. L. Smith and K. M. Black, J. Vac. Sci. Technol. A **2**, 744 (1984).
[7] S. Santavirta, M. Takagi, L. Nordsletten, A. Anttila, R. Lappalainen, and Y. T. Konttinen, Arch. Orthop. Trauma Surg. **118**, 89 (1998).
[8] G. Cicero, A. Catellani, and G. Galli, Phys. Rev. Lett. **93**, 016102 (2004).
[9] V. M. Bermudez, Phys. Status Solidi B **202**, 447 (1997).
[10] J. Pollmann, P. Krüger, and M. Sabisch, Phys. Status Solidi B **202**, 421 (1997).
[11] P. Soukiassian and H. B. Enriquez, J. Phys.: Condens. Matter **16**, S1611 (2004).
[12] K. Heinz, J. Bernhardt, J. Schardt, and U. Starke, J. Phys.: Condens. Matter **16**, S1705 (2004).
[13] Th. Seyller, J. Phys.: Condens. Matter **16**, S1755 (2004).

[14] J. Pollmann and P. Krüger, J. Phys.: Condens. Matter **16**, S1659 (2004).
[15] C. Virojanadara, M. Hetzel, and U. Starke, Appl. Phys. Lett. **92**, 061902 (2008).
[16] C. Virojanadara, M. Hetzel, L. I. Johansson, W. J. Choyke, and U. Starke, Surf. Sci. **602**, 525 (2008).
[17] Y. Shishkin, W. J. Choyke, and R. P. Devaty, J. Appl. Phys. **96**, 2311 (2004).
[18] U. Starke, W. Y. Lee, C. Coletti, S. E. Saddow, R. P. Devaty, and W. J. Choyke, Appl. Phys. Lett. **88**, 031915 (2006).
[19] J. P. Perdew and Y. Wang, Phys. Rev. B **45**, 13244 (1992).
[20] D. R. Hamann, Phys. Rev. B **40**, 2980 (1989).
[21] L. Kleinman and D. M. Bylander, Phys. Rev. Lett. **48**, 1425 (1982).
[22] We use as decay constants (in atomic units) 0.18, 0.50, and 1.00 (0.25, 1.00, and 2.86) for Si (C) atoms of the two outer surface layers as well as the silicon adatom. For the deeper layers of the slab, the decay constants 0.20 and 0.60 (0.35 1.70) are used for Si (C), while ten orbitals with a decay constant of 0.35 are employed for the saturating hydrogen atoms.
[23] J. Wieferink, P. Krüger, and J. Pollmann, Phys. Rev. B **74**, 205311 (2006).
[24] H. J. Monkhorst and J. D. Pack, Phys. Rev. B **13**, 5188 (1976).
[25] B. Baumeier, P. Krüger, and J. Pollmann, Phys. Rev. B **73**, 195205 (2006).
[26] S. K. Burger and W. Yang, J. Chem. Phys. **124**, 054109 (2006).
[27] G. Henkelman and H. Jónsson, J. Chem. Phys. **113**, 9978 (2000).
[28] J. Wieferink, P. Krüger, and J. Pollmann (unpublished).
[29] J. Tersoff and D. R. Hamann, Phys. Rev. B **31**, 805 (1985).
[30] Our calculated lattice constants $a=3.11$ and $c=10.17$ Å overestimate the experimental values (Ref. 1) of 3.07 and 10.05 Å by about 1%, as is usual within GGA. Accordingly, an overestimate of this order occurs in the surface structure parameters, as well.
[31] A. Seubert, J. Bernhardt, M. Nerding, U. Starke, and K. Heinz, Surf. Sci. **454-456**, 45 (2000).
[32] U. Starke, J. Schardt, J. Bernhardt, M. Franke, and K. Heinz, Phys. Rev. Lett. **82**, 2107 (1999).
[33] M. Sabisch, P. Krüger, and J. Pollmann, Phys. Rev. B **55**, 10561 (1997).
[34] J. M. Powers, A. Wander, P. J. Rous, M. A. Van Hove, and G. A. Somorjai, Phys. Rev. B **44**, 11159 (1991).
[35] J. P. Long, V. M. Bermudez, and D. E. Ramaker, Phys. Rev. Lett. **76**, 991 (1996).
[36] H. W. Yeom, M. Shimomura, J. Kitamura, S. Hara, K. Tono, I. Matsuda, B. S. Mun, W. A. R. Huff, S. Kono, T. Ohta, S. Yoshida, H. Okushi, K. Kajimura, and C. S. Fadley, Phys. Rev. Lett. **83**, 1640 (1999).
[37] P. Käckell, J. Furthmüller, F. Bechstedt, G. Kresse, and J. Hafner, Phys. Rev. B **54**, 10304 (1996).
[38] A. Catellani, G. Galli, and F. Gygi, Phys. Rev. Lett. **77**, 5090 (1996).
[39] M. Sabisch, P. Krüger, A. Mazur, M. Rohlfing, and J. Pollmann, Phys. Rev. B **53**, 13121 (1996).
[40] A. Catellani, G. Galli, and P. L. Rigolli, Phys. Rev. B **62**, R4794 (2000).
[41] F.-H. Wang, P. Krüger, and J. Pollmann, Phys. Rev. B **66**, 195335 (2002).
[42] M. J. Litzkow, M. Livny, and M. W. Mutka, *Proceedings of the Eighth International Conference on Distributed Computing Systems* (IEEE, Washington, D.C., 1988), pp. 104–111.
[43] J. P. Perdew and A. Zunger, Phys. Rev. B **23**, 5048 (1981).
[44] R. Ostendorf, C. Benesch, M. Hagedorn, H. Merz, and H. Zacharias, Phys. Rev. B **66**, 245401 (2002).